HMG Advance Access published October 16, 2007

The Angelman syndrome ubiquitin ligase localizes to the synapse and nucleus, and maternal deficiency results in abnormal dendritic spine morphology.

Scott V. Dindot[1], Barbara A. Antalffy[1,2], Meenakshi B. Bhattacharjee[2], and Arthur L. Beaudet[1*]

[1]Department of Molecular and Human Genetics, [2]Department of Pathology, Baylor College of Medicine, One Baylor Plaza, Houston TX, 77030

*Correspondence should be addressed to Arthur L. Beaudet
One Baylor Plaza
Baylor College of Medicine
Houston TX, 77030
713-798-4795 (Phone)
713-798-7773 (Fax)
(abeaudet@bcm.tmc.edu)

ABSTRACT

Loss of function of the maternally inherited allele for the *UBE3A* ubiquitin ligase gene causes Angelman syndrome (AS), which is characterized by severe neurological impairment and motor dysfunction. In addition, *UBE3A* lies within chromosome 15q11-q13 region where maternal, but not paternal, duplications cause autism. The *UBE3A* gene product, E6-AP, has been shown to function both as an E3 ligase in the ubiquitin proteasome pathway and as a transcriptional coactivator. However, the specific role of E6-AP in the brain, or how loss of function of E6-AP results in AS is unclear. Herein, we show, using a recombinant transgenic mouse expressing a *Ube3a*^{YFP} fusion gene, that the maternal *Ube3a*^{YFP} allele is upregulated and preferentially expressed in neurons, and that the fusion protein, E6-AP:YFP, is enriched in the nucleus and dendrites *in vivo*. We also show that E6-AP:YFP localizes to the nucleus and to presynaptic and postsynaptic compartments in cultured hippocampal neurons. Furthermore, we show that cerebellar Purkinje cell number and dendritic branching are not affected in *Ube3a* maternal deficient mice, but that dendritic spine development, including spine morphology, number, and length, are affected on cerebellar Purkinje cells, and on pyramidal neurons in the hippocampus and cortex. Collectively, these data suggest that the neurological deficits observed in AS patients and in AS mice may result from specific abnormalities in synaptic development and/or plasticity.

INTRODUCTION

Angelman syndrome (AS) is characterized by severe mental retardation, absence of speech, ataxia, and a happy disposition (1, 2). The AS gene, *UBE3A*, encodes the E6-AP ubiquitin ligase and is subject to genomic imprinting with preferential maternal specific expression in brain and more specifically in neurons but not glia (3, 4). Maternal but not paternal interstitial duplications of chromosome 15q11-q13 cause autism (5). These duplications encompass multiple genes, but *UBE3A* is a strong candidate to contribute to the autism phenotype in 15q11-q13 duplication cases based on its imprinted status and known causative role in AS (6). Autism spectrum disorders are seen with Prader-Willi syndrome and AS, the two phenotypes associated with paternal and maternal deletions of 15q11-q13, respectively (7, 8).

Mice with a maternal null mutation in *Ube3a* (AS mice) have defects in long term potentiation (LTP) and manifest motor and behavioral abnormalities that parallel findings in AS in spite of normal cellular architecture in the brain (9) . The neurological deficits in AS mice have been directly linked to the postsynaptic calcium/calmodulin kinase type 2 (CaMKII) signaling pathway, as AS mice have increased inhibitory phosphorylation of αCaMKII in the brain (10). Moreover, the learning and behavioral deficits present in AS mice can be rescued through a mutation in CaMKII that prevents its inhibitory phosphorylation (11). Other reports have linked E6-AP to various neurologically relevant proteins including epithelial cell transforming sequence 2 oncogene (Ect2) (12), neuronal protein interacting specifically with TC10 (nPIST) (13), and myc binding protein-2 (MYCBP2) (Drosophila ortholog of Highwire) (14), although the functional relevance of these interactions is unclear.

The AS protein, E6-AP, has three isoforms that differ at the N-terminus (15), is a multifunctional E3 ubiquitin ligase, and has transcriptional coactivator activity (16); some

targets of ubiquitination are known (e.g., p53 oncoprotein), but none have shed light on the AS phenotype or the function of E6-AP in the brain. Although *Ube3a* is highly expressed in neurons based on *in situ* hybridization studies, the subcellular localization of E6-AP remains unclear, particularly as it relates the dual transcriptional coactivator and ubiquitin ligase activities, whether effects on CaMKII are direct or indirect, and how its deficiency causes the AS phenotype.

Here we show using a knock-in *Ube3a*^{YFP} fusion reporter mouse, that *Ube3a*^{YFP} is expressed preferentially from the maternal allele in central neurons but is biallelicly expressed in glial cells, and that the E6-AP:YFP fusion protein localizes both to the nucleus and to the synapse. In addition, we show that mice with maternal deficiency for *Ube3a* have abnormal dendritic spine morphology and density.

RESULTS

Generation of *Ube3a*^{YFP} reporter mice.

In order to examine the cell type parental allelic expression of *Ube3a* and to elucidate the cellular localization of the *Ube3a* gene product, E6-AP, we produced mice with a knock-in mutation fusing YFP to the C-terminus of E6-AP (**Fig. 1A – C**; targeted allele, *Ube3a*^{YFP}; fusion protein, E6-AP:YFP). The *Ube3a*^{YFP} mice were mated to wild-type (WT) mice to obtain offspring that inherited the *Ube3a*^{YFP} allele either through the maternal or paternal germline. Based on the increased molecular weight of E6-AP:YFP (E6-AP, 100 kDa; E6-AP:YFP, 130 kDa), we used western blotting to distinguish expression of the *Ube3a*^{YFP} allele according to parent-of-origin. Cerebellar lysates from mice inheriting the *Ube3a*^{YFP} allele maternally, but not paternally, revealed an increase in the molecular weight of E6-AP indicating preferential maternal expression of the *Ube3a*^{YFP} allele (**Fig. 1D**). Maternal specific expression of *Ube3a*^{YFP} in cerebellum was

further confirmed with an anti-YFP antibody (**Fig. 1D**). Moreover, the amount of E6-AP:YFP fusion protein detected by western blot was consistent with the levels of endogenous E6-AP protein, indicating that expression of *Ube3a*^{YFP} was not grossly altered by the generation of the fusion protein(**Fig 1D**). In addition, studies with multiple antibodies to E6-AP in wild-type mice were consistent with the distribution patterns seen with the fusion protein (data not shown).

Analysis of *Ube3a*^{YFP} allelic expression and cellular localization *in vivo*.

Next, we examined cell type of expression of *Ube3a*^{YFP} according to parent-of-origin, and the subcellular localization of E6-AP:YFP in the brain using confocal imaging. Frozen sections from adult *Ube3a*^{YFP} maternal and *Ube3a*^{YFP} paternal brains were immunostained with anti-YFP and anti-GFAP, a glial cell marker, or anti-YFP and anti-calbindin, a cerebellar Purkinje cell marker. *Ube3a*^{YFP} maternal mice exhibited high levels of expression in the cortical and hippocampal pyramidal neurons (**Fig. 2A, D**), whereas expression was only faintly detected in the corresponding regions in *Ube3a*^{YFP} paternal mice (**Fig. 2A**). In the cerebellum, *Ube3a*^{YFP} was expressed in Purkinje cells and in neurons in the granular and molecular layers, although at lower levels (**Fig 2B**). Biallelic expression of *Ube3a*^{YFP} was detected in GFAP positive cells lining the lateral ventricles, although each allele was expressed at levels lower than seen with expression of the maternal allele in neurons in the CA3 region of the hippocampus (**Fig. 2C**). Biallelic expression was limited to GFAP positive cells lining the ventricles, including the third ventricle (data not shown), and was not readily detectable in GFAP positive astrocytes in other brain regions. Expression of maternal derived *Ube3a*^{YFP} was detected in most brain regions including hippocampus, cortex, thalamus, olfactory bulb and cerebellum. *Ube3a*^{YFP} paternal expression was only faintly detected in these and other brain regions, aside for the expression detected in GFAP positive cells lining the

ventricles. For each neuronal cell population, E6-AP:YFP localized primarily to the nucleus, but was additionally present in the soma and dendrites as is clearly seen in pyramidal, Purkinje, and olfactory bulb neurons (**Fig. 2D, E, and F**). These data indicate that *Ube3a*^{YFP} undergoes preferential abundant expression of the maternal allele exclusively in neurons and that E6-AP:YFP localizes to nucleus, cytoplasm of the cell body, and processes in these cells.

E6-AP:YFP localizes to both presynaptic and postsynaptic compartments in dissociated hippocampal neurons in culture.

Since E6-AP:YFP was enriched in the nuclei of neurons, and was additionally present in cell body and dendrites, as seen in hippocampal CA1 pyramidal neurons (**Fig. 2D**), we next analyzed the subcellular localization of E6-AP:YFP in dissociated hippocampal neurons developing in culture derived from mice with a maternally inherited *Ube3a*^{YFP} allele. Hippocampal neurons at 1-4 days *in vitro* (DIV) exhibited high levels of E6-AP:YFP in the growth cones of developing neurites and in the nucleus (**Fig. 3A**). At 4 DIV, anti-MAP2 was used to stain dendrites, and high levels of E6-AP:YFP were detected in the growth cones of both axons and dendrites (**Fig. 3B**). In order to examine whether E6-AP:YFP was present at the synapse, we analyzed *Ube3a*^{YFP} neurons cultured for 25 DIV and double stained with anti-synaptophysin, a presynaptic vesicle marker, and anti-YFP. E6-AP:YFP was highly enriched in the nucleus, and was present along axons and dendrites. Images of axons indicated that E6-AP:YFP colocalized with synaptophysin as distinct puncta along axons (**Fig. 3C**). In dendrites, a different pattern of staining was observed with E6-AP:YFP being diffusely distributed and not forming distinct puncta. However, E6-AP:YFP was detected in spine like protrusions along dendritic shafts, some exhibiting positive and negative staining for synaptophysin (**Fig. 3D**). Collectively, these results indicate that E6-AP:YFP differentially localizes to the

nucleus, growth cone, and synapse, including presynaptic and postsynaptic compartments, in hippocampal neurons in culture, suggesting that E6-AP may directly regulate development and/or function of synapses.

Cerebellar Purkinje cell number and dendritic branching are not affected by loss of maternal E6-AP

We next evaluated cerebellar Purkinje cell number and dendritic branching, in *Ube3a* maternal deficient mice (AS mice) (9, 17). We analyzed the integrity of cerebellar Purkinje cells in WT and AS mice by examining organization, cell number, and dendritic branching through calbindin staining, which immunolabels Purkinje cell soma and dendrites. The distribution and organization of Purkinje cells in AS mice was similar to WT with no obvious differences being apparent at the light microscope level. Furthermore, we did not detect any differences in Purkinje cell number between WT and AS mice (WT, 11.98 ± 0.83/250 μm PC layer; AS, 11.64 ± .19/250 μm; P = 0.7), nor did we detect any differences in calbindin staining of dendritic trees, which is an indirect indicator of Purkinje cell dendritic density and branching (**Fig 4 A**) (18). These observations are consistent with previous reports (9, 19). In other regions in the brain where there were no apparent abnormalities observed by immunohistochemical analysis. Therefore, these data indicate that the neurological deficits observed in AS mice do not arise from abnormalities involving Purkinje cell number or dendritic branching.

AS mice have abnormal dendritic spines on cerebellar Purkinje cells and hippocampal and cortical pyramidal neurons.

Given the presence of E6-AP:YFP in dendrites *in vivo* and at synapses in cultured neurons, we performed Golgi staining in WT and AS mice in order to examine

dendritic spine morphology and density. Brains from adult wild-type and AS littermates were extracted and Golgi impregnated. Corresponding sections from wild-type and AS mice were examined by light microscopy. Images revealed that dendritic spines along Purkinje cells, hippocampal pyramidal, and cortical pyramidal neurons in WT mice appeared “mushroom like” with large heads and thin, short necks studded along dendrites. In contrast, spines in AS mice displayed an inconsistent morphology, including high variability in spine neck length and head size. The density of spines also appeared lower in AS mice compared to WT mice (**Fig. 5A**). Because the high density and crowding of spines in Purkinje cells made detailed analysis difficult, we quantified dendritic spines in hippocampal and cortical pyramidal neurons (**Fig. 5A**). Secondary apical dendrites close to the cell soma and extending horizontally from pyramidal neurons in the CA1 region were analyzed for dendritic spine density and length in WT and AS mice. Quantification revealed that AS mice showed a significant reduction in spine density compared to WT mice (WT, 1.614± 0.076 spines/μm; AS, 1.228 ±0.055 spines/μm; P = 0.0003; **Fig. 5B**). A reduction in spines along cortical apical dendrites was also observed in AS mice (WT, 1.172 ± 0.044 spines/μm; AS, 0.882 ± 0.057 spines/μm; P = 0.0009; **Fig. 5C**). We next quantified spine lengths in hippocampal dendrites, and AS mice exhibited a significant reduction in the overall average spine length compared to WT (WT, 1.16 ± 0.0038 μm; AS, 1.017 ± 0.0454 μm; P = 0.03; **Fig. 5D**). The pyramidal dendrites in AS mice also exhibited varicosities along the secondary dendritic shaft (**Fig. 5A**). In addition, many of the dendrites appeared thinner in AS mice relative to WT. Collectively, these data indicate that loss of maternal E6-AP results in abnormal dendritic spine development, and may underlie the deficits in functional synaptic plasticity observed in AS mice.

Discussion

In the present study, we examined the cell type expression and subcellular localization of E6-AP in the brain through an *Ube3a*^{YFP} knock-in fusion reporter mouse. In addition, we examined the brains of AS mice for yet undetected morphological phenotypes associated with the neurological deficits present in these mice. Our results indicate that *Ube3a* is highly expressed from the maternal allele specifically in neurons, and that E6-AP differentially localizes to the nucleus and synapse, where it may act locally to regulate synaptic development and plasticity.

Previous studies have indicated that the mouse *Ube3a* gene undergoes genomic imprinting with preferential expression of the maternal allele in central neurons in the brain (3, 4, 17). Our results are consistent with these previous observations, and demonstrate through *in vivo* analyses, that the paternal allele is expressed at very low to undetectable levels in neurons, whereas both alleles are expressed approximately equally in glial cells lining the ventricles. Notably, we observed an upregulation of the maternal allele in neurons relative to the maternal allele expressed in glial cells with biallelic expression. We also observed that E6-AP:YFP was differentially localized between the nucleus and cell body soma, extending to the growth cone and presynaptic and postsynaptic compartments in hippocampal neurons in culture. These findings support a diverse role for E6-AP as an ubiquitin ligase and transcriptional coactivator.

Our observations that AS mice have a normal cellular architecture in the brain, but possess dendritic spines that are abnormally shaped, and reduced in size and density suggests that E6-AP does not regulate neurogenesis *per se*, but may function locally to regulate spine development or synaptic plasticity. The presence of E6-AP at the synapse further supports this idea (20), although we cannot exclude a possible

contribution of a nuclear role for E6-AP in regulating the structure and/or function of the synapse. Consistent with other mouse models for mental retardation, such as fragile X and Rett syndromes, AS mice clearly possess altered spine morphologies. *Fmr1* null mice and fragile X patients have been shown to possess abnormally long dendritic spines as well as increased dendritic spine densities in various neuronal populations (21-27). In contrast, *MeCP2* deficient mice and Rett patients have been shown to exhibit reduced dendritic spine densities (28-30). Consistent with our observations in AS mice, *Fmr1* and *MeCP2* null mice possess apparently normal neuronal maturation and arborization, but manifest abnormal synapse development.

Although there have been no specific targets of E6-AP ubiquitination identified to date that would contribute to our understanding of E6-AP synaptic function, there is evidence for effects on the CaMKII pathway. Studies in AS mice have shown that deficiency of *Ube3a* results in increased inhibitory phosphorylation and reduced postsynaptic density (PSD) associated CaMKII (10). Further studies have shown rescue of the AS behavioral phenotypes in CaMKII mutants by introducing an additional mutation at the inhibitory phosphorylation site of αCaMKII, therefore demonstrating dysregulation of CaMKII is likely the underlying molecular basis for the long term potentiation deficits (11). Consistent with our findings of abnormal dendritic spines in AS mice, CaMKII has been shown to play an important role in both functional and structural synaptic plasticity. Induction of activated CaMKII results in new filopodia growth and spine formation, whereas inhibition of CaMKII activity results in filopodia and spine loss (31). Therefore, loss of E6-AP and the subsequent dysregulation of CaMKII, likely leads to impairments in both functional and structural synaptic plasticity.

There is other evidence that is consistent with an important role for E6-AP at the synapse. E6-AP has been shown to interact with MYCBP2, the human ortholog of

Drosophila Highwire which is known to regulate synaptic development and function (14, 32, 33). Given the lack of any apparent organizational or cellular defects in AS mice and the presence of E6-AP at the synapse, we predict that the loss of synaptic E6-AP and the resulting abnormal morphology of dendritic spines in AS mice contributes partially, if not entirely, to the neurological deficits observed in these mice and possibly in AS individuals.

MATERIALS AND METHODS

Generation of *Ube3a*^{YFP} mice.

Genomic DNA from the 129/SvEv mouse strain was used as a template to PCR amplify an 8.88-kb fragment of the 3´-end of *Ube3a* including intron 8, exon 9, intron 9, exon 10, and the 3´-UTR (F:5´-GTTTCGTCACTTCTTTCTTCCGCTC; R:5´-TGTTAGTTTCCAATGCCTCCTACGC). The PCR fragment was TA cloned into the TOPO-XL vector (Invitrogen, Carlsbad CA). The homology arms were digested at an *Sph*I site that is located eight nucleotides upstream of the *Ube3a* translational stop codon. A linker, which contained the 3´-end of the coding sequence without the translational stop but with an *Xho*I restriction site, was ligated into the *Sph*I site (F:5´-CTGTTCTCGAGGAATTCCGCGGTCATG, R:5´-ACCGCGGAATTCCTCGAGAACAGCATG) . An EYFP: loxP: PGK-Neomycin: loxP cassette was ligated into the *Xho*I site allowing for in frame fusion of the EYFP gene to the full-length *Ube3a*. The *Ube3a*^{YFP} targeting construct was linearized and electroporated into AB2.2 ES cells as described previously (9) . G418 resistant clones were screened by Southern blotting using a 5´-PCR probe (F:5´-GGACTTTGCTTGGTGTTGGT, R:5´-GGAAGTCAGAAGGGGGAA) and 3´-PCR probe (F:5´-GGGTCTTTTGAGTTGCGGTA, R:5´-TCATCTGTCCCAGGGAAAAC). One

positive clone was expanded and confirmed for homologous recombination by a second round of Southern blotting using the same 5´- and 3´-probes. The targeted clone was injected into albino C57/BL6 blastocysts by standard procedures. Three low to medium percentage chimeras were bred to C57/BL6 and germline transmission of the *Ube3a*^{YFP} allele was determined by agouti coat color and Southern blot. The *Ube3a*^{YFP} genotype was maintained on a mixed 129/SvEv and C57/BL6 background.

Western blot analysis

Mice were sacrificed and brains immediately isolated and transferred to ice cold PBS. Brain tissues were dissected out and immediately transferred to tubes containing ice cold NP40/SDS buffer (1% Nonidet P-40, 0.01% SDS, 0.1M Tris-HCl, pH 7.2) and complete Protease Inhibitor Cocktail (Roche Applied Sciences, Indianapolis, IN) and homogenized with a motorized pestle. The lysates was rotated for 15 min at 4ºC, centrifuged at 14,000 RPM for 15 minutes to remove insoluble proteins, and then transferred to fresh tubes and put on ice. This was repeated and supernatants were combined into one tube. Protein concentrations were determined using the Bradford reagent (Bio-Rad, Hercules, CA).

Brain tissue homogenates were resolved on a 7.5% SDS-PAGE gel and transferred to a TransBlot nitrocellulose membrane (Bio-Rad). The membranes were blocked in 3% non-fat milk in 0.1 % T-TBS (10 mM Tris-HCl pH 7.5, 150 mM NaCl, and 0.1% Tween-20) for 1 hr at room temperature. The membranes were incubated in the primary antibody for 1 hr at room temperature and then washed 3 times with T-TBS. The membrane was then incubated in secondary antibody for 1 hr at room temperature. The membranes were washed again 3 times in T-TBS before being developed by enhanced chemiluminescence method (Amersham, Piscataway, NJ). Anti-GFP was diluted at 1:3000 (8371; BD Bioscience, San Jose, CA) and anti-E6-AP (611416; BD Bioscience) was diluted at 1:1000. Secondary antibodies were diluted at 1:3000.

Hippocampal neuronal culture

Primary cultures of hippocampal neurons were obtained from P0-P1 pups of C57/BL6 males crossed to *Ube3a*^{YFP} females. Hippocampi were dissociated with papain and cultured in a chemically defined medium (Neurobasal medium A; Invitrogen, San Diego, CA) supplemented with B27 (Invitrogen) and Penicillin/Streptomycin (Invitrogen) on glass coverslips coated with Poly-D-Lysine (Sigma) and collagen (BD Biosciences, San Jose, CA) as previously reported (34) . Cultures were maintained at 37ºC in 5% CO_2 until use.

Immunostaining

Mice were perfused with ice cold PBS and 4% paraformaldehyde and tissues harvested as described previously (35) . For frozen sections, 45 µm coronal sections were cut on a cryostat and stored in PBS. Sections were washed in PBS and then blocked in T-TBS (10mM Tris-HCl pH7.5, 0.3% TritonX-100) plus 5% normal goat serum for 1-2 hr at 4ºC. Sections were incubated in primary antibody for 48-72 hr at 4ºC in a humidified chamber with gentle agitation. Anti-GFP (NB 600-308; Novus Biologicals, Littleton, CO) was used at 1:2000 dilution, anti-GFAP (MAB360; Chemicon, Temecula, CA) at 1:250, and anti-calbindin (C9848; Sigma) at 1:500. Sections were washed three times in T-TBS for 10 minutes each and then incubated with a fluorescently labeled secondary antibodies (Jackson ImmunoResearch, West Grove, PA) for 24 h at 4ºC in the dark. Anti-rabbit Alexa 488 was used at 1:200, anti-mouse Alexa 557 was used at 1:200 (Invitrogen). Sections were washed again in T-TBS for 20 minutes each and mounted on glass slides with Vectashield (Vector Laboratories, Burlingame, CA) mounting reagent. Confocal images were obtained using an LSM 510 Zeiss confocal microscope (Zeiss, Oberkochen, Germany).

Immunostaining data analysis

Ube3a^{YFP} parental expression. All images were acquired on a Zeiss LSM 510 confocal microscope with a 10X or 43X oil immersed objective. The detector and amplifier gain exposure settings were kept the same between sample groups. For anti-GFP fluorescence in *Ube3a^{YFP}* maternal and *Ube3a^{YFP}* paternal mice, wild-type sections were imaged in order to determine the maximum laser intensity and detector gain below the threshold level of fluorescence detection. *Ube3a^{YFP}* maternal and *Ube3a^{YFP}* paternal sections were then scanned using these imaging conditions.

Purkinje cell dendritic arborization. For Purkinje cell dendritic arborization, 45 μm cryosections from six week old WT (n=2) and AS (n=2) sex matched littermates were immunostained with anti-calbindin (1:500). All images were acquired on a Zeiss confocal microscope using the 43X objective. The same folia and approximate depth of section were analyzed for each animal. Images were acquired from the Purkinje cell soma extending to the distal end of dendritic branches in the molecular cell layer. Twenty-five sequential, 0.5 μm thick optical images were acquired and were projected using the NIH ImageJ Z-projection function set for average intensity. For each genotype, a 20 μm X 160 μm rectangular section centered on an individual PC soma was selected from the same region from each animal. The fluorescence intensity profile of this region was calculated using the plot profile in ImageJ. Mean fluorescence (n=5) for the optical section was calculated every 2.25 μm along PC soma and dendrites. Student's t-test was performed on the mean fluorescence for the entire optical section ($P = 0.421$) and on the mean dendritic fluorescence ($P = 0.437$).

Dendritic spine analysis

Golgi impregnation was performed according to the protocol outlined in the FD Rapid GolgiStain Kit (FD Neurotechnologies, Ellicott, MD). One-hundred μm serial sections of the cerebellum and hippocampus were cut and mounted. Images were

acquired using a Zeiss (Zeiss Imager. Z.1) light microscope. For dendritic spine density and length measurements, 30-40 serial z-stacked images spanning the entire dendrite and protruding spines (0.36 μm/image) were acquired using a 100X oil immersion lens. For hippocampal pyramidal neurons, 6-7 secondary dendrites branching from the apical dendrite and most proximal to the cell body soma were imaged per animal. For cortical pyramidal neurons, 5-6 apical dendrites, approximately 100 μm from the cell body soma, were imaged per animal. Serial images were analyzed using NIH ImageJ software. Spine density and length were quantified by focusing through each serial image, and counts and measurements were made using the measurement function. For images, 20-25 z-stacked images were projected through deconvolution software. Seven to eight week old male and female WT (n=3) and AS (n=3) littermate mice were used for analysis.

Statistics

Microsoft Excel was used for statistical analysis. For wild-type and AS comparisons, student's t-test was used to determine statistical significance. All data represents mean ± standard error of the mean (SEM). A student's t-test with a value of $P < 0.05$ was considered significant (individual P values are indicated by an asterisk in the figures).

ACKNOWLEDGEMENTS

The authors thank Drs. Huda Y. Zoghbi, Hugo J. Bellen, and Kim Tolias for critical reading of the manuscript. S.V.D and A.L.B are supported by grants from the National Institutes of Health (F32 HD-049248; R01 HD-037283). This work was supported by Baylor College of Medicine Mental Retardation and Developmental Disabilities Research Center (MRDDRC) NIH grant HD-24064.

REFERENCES

1. Lossie, A.C., Whitney, M.M., Amidon, D., Dong, H.J., Chen, P., Theriaque, D., Hutson, A., Nicholls, R.D., Zori, R.T., Williams, C.A. *et al.* (2001) Distinct phenotypes distinguish the molecular classes of Angelman syndrome. *J. Med. Genet.,* **38,** 834-845.
2. Williams, C.A., Beaudet, A.L., Clayton-Smith, J., Knoll, J.H., Kyllerman, M., Laan, L.A., Magenis, R.E., Moncla, A., Schinzel, A.A., Summers, J.A. *et al.* (2006) Angelman syndrome 2005: updated consensus for diagnostic criteria. *Am. J. Med. Genet. A,* **140,** 413-418.
3. Albrecht, U., Sutcliffe, J.S., Cattanach, B.M., Beechey, C.V., Armstrong, D., Eichele, G. and Beaudet, A.L. (1997) Imprinted expression of the murine Angelman syndrome gene, Ube3a, in hippocampal and Purkinje neurons. *Nat. Genet.,* **17,** 75-78.
4. Yamasaki, K., Joh, K., Ohta, T., Masuzaki, H., Ishimaru, T., Mukai, T., Niikawa, N., Ogawa, M., Wagstaff, J. and Kishino, T. (2003) Neurons but not glial cells show reciprocal imprinting of sense and antisense transcripts of Ube3a. *Hum. Mol. Genet.,* **12,** 837-847.
5. Cook, E.H., Jr., Lindgren, V., Leventhal, B.L., Courchesne, R., Lincoln, A., Shulman, C., Lord, C. and Courchesne, E. (1997) Autism or atypical autism in maternally but not paternally derived proximal 15q duplication. *Am. J. Hum. Genet.,* **60,** 928-934.
6. Jiang, Y.H., Sahoo, T., Michaelis, R.C., Bercovich, D., Bressler, J., Kashork, C.D., Liu, Q., Shaffer, L.G., Schroer, R.J., Stockton, D.W. *et al.* (2004) A mixed epigenetic/genetic model for oligogenic inheritance of autism with a limited role for UBE3A. *Am. J. Med. Genet. A,* **131,** 1-10.
7. Veltman, M.W., Craig, E.E. and Bolton, P.F. (2005) Autism spectrum disorders in Prader-Willi and Angelman syndromes: a systematic review. *Psychiatr. Genet.,* **15,** 243-254.
8. Bonati, M.T., Russo, S., Finelli, P., Valsecchi, M.R., Cogliati, F., Cavalleri, F., Roberts, W., Elia, M. and Larizza, L. (2007) Evaluation of autism traits in Angelman syndrome: a resource to unfold autism genes. *Neurogenetics*.
9. Jiang, Y.H., Armstrong, D., Albrecht, U., Atkins, C.M., Noebels, J.L., Eichele, G., Sweatt, J.D. and Beaudet, A.L. (1998) Mutation of the Angelman ubiquitin ligase in mice causes increased cytoplasmic p53 and deficits of contextual learning and long-term potentiation. *Neuron,* **21,** 799-811.
10. Weeber, E.J., Jiang, Y.H., Elgersma, Y., Varga, A.W., Carrasquillo, Y., Brown, S.E., Christian, J.M., Mirnikjoo, B., Silva, A., Beaudet, A.L. *et al.* (2003) Derangements of hippocampal calcium/calmodulin-dependent protein kinase II in a mouse model for Angelman mental retardation syndrome. *J. Neurosci.,* **23,** 2634-2644.
11. van Woerden, G.M., Harris, K.D., Hojjati, M.R., Gustin, R.M., Qiu, S., de Avila Freire, R., Jiang, Y.H., Elgersma, Y. and Weeber, E.J. (2007) Rescue of

neurological deficits in a mouse model for Angelman syndrome by reduction of alphaCaMKII inhibitory phosphorylation. *Nat. Neurosci.,* **10,** 280-282.

12. Reiter, L.T., Seagroves, T.N., Bowers, M. and Bier, E. (2006) Expression of the Rho-GEF Pbl/ECT2 is regulated by the UBE3A E3 ubiquitin ligase. *Hum. Mol. Genet.,* **15,** 2825-2835.
13. Jeong, K.W., Kim, H.Z., Kim, S., Kim, Y.S. and Choe, J. (2007) Human papillomavirus type 16 E6 protein interacts with cystic fibrosis transmembrane regulator-associated ligand and promotes E6-associated protein-mediated ubiquitination and proteasomal degradation. *Oncogene,* **26,** 487-499.
14. Jung, S.Y., Malovannaya, A., Wei, J., O'Malley, B.W. and Qin, J. (2005) Proteomic analysis of steady-state nuclear hormone receptor coactivator complexes. *Mol. Endocrinol.,* **19,** 2451-2465.
15. Yamamoto, Y., Huibregtse, J.M. and Howley, P.M. (1997) The human E6-AP gene (UBE3A) encodes three potential protein isoforms generated by differential splicing. *Genomics,* **41,** 263-266.
16. Nawaz, Z., Lonard, D.M., Smith, C.L., Lev-Lehman, E., Tsai, S.Y., Tsai, M.J. and O'Malley, B.W. (1999) The Angelman syndrome-associated protein, E6-AP, is a coactivator for the nuclear hormone receptor superfamily. *Mol. Cell. Biol.,* **19,** 1182-1189.
17. Miura, K., Kishino, T., Li, E., Webber, H., Dikkes, P., Holmes, G.L. and Wagstaff, J. (2002) Neurobehavioral and electroencephalographic abnormalities in Ube3a maternal-deficient mice. *Neurobiol. Dis.,* **9,** 149-159.
18. Bowman, A.B., Lam, Y.C., Jafar-Nejad, P., Chen, H.K., Richman, R., Samaco, R.C., Fryer, J.D., Kahle, J.J., Orr, H.T. and Zoghbi, H.Y. (2007) Duplication of Atxn1l suppresses SCA1 neuropathology by decreasing incorporation of polyglutamine-expanded ataxin-1 into native complexes. *Nat. Genet.,* **39,** 373-379.
19. Cummings, C.J., Reinstein, E., Sun, Y., Antalffy, B., Jiang, Y., Ciechanover, A., Orr, H.T., Beaudet, A.L. and Zoghbi, H.Y. (1999) Mutation of the E6-AP ubiquitin ligase reduces nuclear inclusion frequency while accelerating polyglutamine-induced pathology in SCA1 mice. *Neuron,* **24,** 879-892.
20. Colledge, M., Snyder, E.M., Crozier, R.A., Soderling, J.A., Jin, Y., Langeberg, L.K., Lu, H., Bear, M.F. and Scott, J.D. (2003) Ubiquitination regulates PSD-95 degradation and AMPA receptor surface expression. *Neuron,* **40,** 595-607.
21. Irwin, S.A., Patel, B., Idupulapati, M., Harris, J.B., Crisostomo, R.A., Larsen, B.P., Kooy, F., Willems, P.J., Cras, P., Kozlowski, P.B. *et al.* (2001) Abnormal dendritic spine characteristics in the temporal and visual cortices of patients with fragile-X syndrome: a quantitative examination. *Am. J. Med. Genet.,* **98,** 161-167.
22. Grossman, A.W., Elisseou, N.M., McKinney, B.C. and Greenough, W.T. (2006) Hippocampal pyramidal cells in adult Fmr1 knockout mice exhibit an immature-appearing profile of dendritic spines. *Brain. Res.,* **1084,** 158-164.
23. McKinney, B.C., Grossman, A.W., Elisseou, N.M. and Greenough, W.T. (2005) Dendritic spine abnormalities in the occipital cortex of C57BL/6 Fmr1 knockout mice. *Am. J. Med. Genet. B Neuropsychiatr. Genet.,* **136,** 98-102.
24. Koekkoek, S.K., Yamaguchi, K., Milojkovic, B.A., Dortland, B.R., Ruigrok, T.J., Maex, R., De Graaf, W., Smit, A.E., VanderWerf, F., Bakker, C.E. *et al.* (2005) Deletion of FMR1 in Purkinje cells enhances parallel fiber LTD, enlarges spines, and attenuates cerebellar eyelid conditioning in Fragile X syndrome. *Neuron,* **47,** 339-352.

25. Nimchinsky, E.A., Oberlander, A.M. and Svoboda, K. (2001) Abnormal development of dendritic spines in FMR1 knock-out mice. *J. Neurosci.,* **21,** 5139-5146.
26. Comery, T.A., Harris, J.B., Willems, P.J., Oostra, B.A., Irwin, S.A., Weiler, I.J. and Greenough, W.T. (1997) Abnormal dendritic spines in fragile X knockout mice: maturation and pruning deficits. *Proc. Natl. Acad. Sci. U S A,* **94,** 5401-5404.
27. Hinton, V.J., Brown, W.T., Wisniewski, K. and Rudelli, R.D. (1991) Analysis of neocortex in three males with the fragile X syndrome. *Am. J. Med. Genet.,* **41,** 289-294.
28. Moretti, P., Levenson, J.M., Battaglia, F., Atkinson, R., Teague, R., Antalffy, B., Armstrong, D., Arancio, O., Sweatt, J.D. and Zoghbi, H.Y. (2006) Learning and memory and synaptic plasticity are impaired in a mouse model of Rett syndrome. *J. Neurosci.,* **26,** 319-327.
29. Belichenko, P.V. and Dahlstrom, A. (1995) Studies on the 3-dimensional architecture of dendritic spines and varicosities in human cortex by confocal laser scanning microscopy and Lucifer yellow microinjections. *J. Neurosci. Methods,* **57,** 55-61.
30. Armstrong, D.D. (2001) Rett syndrome neuropathology review 2000. *Brain. Dev.,* **23 Suppl 1,** S72-76.
31. Jourdain, P., Fukunaga, K. and Muller, D. (2003) Calcium/calmodulin-dependent protein kinase II contributes to activity-dependent filopodia growth and spine formation. *J. Neurosci.,* **23,** 10645-10649.
32. Collins, C.A., Wairkar, Y.P., Johnson, S.L. and DiAntonio, A. (2006) Highwire restrains synaptic growth by attenuating a MAP kinase signal. *Neuron,* **51,** 57-69.
33. Wan, H.I., DiAntonio, A., Fetter, R.D., Bergstrom, K., Strauss, R. and Goodman, C.S. (2000) Highwire regulates synaptic growth in Drosophila. *Neuron,* **26,** 313-329.
34. Han, W., Rhee, J.S., Maximov, A., Lin, W., Hammer, R.E., Rosenmund, C. and Sudhof, T.C. (2005) C-terminal ECFP fusion impairs synaptotagmin 1 function: crowding out synaptotagmin 1. *J. Biol. Chem.,* **280,** 5089-5100.
35. Watase, K., Weeber, E.J., Xu, B., Antalffy, B., Yuva-Paylor, L., Hashimoto, K., Kano, M., Atkinson, R., Sun, Y., Armstrong, D.L. *et al.* (2002) A long CAG repeat in the mouse Sca1 locus replicates SCA1 features and reveals the impact of protein solubility on selective neurodegeneration. *Neuron,* **34,** 905-919.

FIGURE LEGENDS.

Figure 1 Generation of *Ube3a*^{YFP} reporter mice. (**A**). Schematic illustration of the *Ube3a* genomic locus (top), *Ube3a*^{YFP} targeting construct (TC, middle), and *Ube3a*^{YFP} targeted allele (bottom). An *Sph*I restriction site located upstream of the translational stop codon was used to remove the stop codon and to fuse the YFP reporter gene to the C-terminus of E6-AP. (**B**) Southern blot analysis of wild type (+/+) and *Ube3a*^{YFP} [E6-AP:YFP (EY) EY/+] positive ES cells. DNA was digested with *Eco*RV and hybridized with the left arm (LA) probe shown in **A**. The fragment sizes for wild type (+/+) and EY (EY/+) alleles are 9.0 kb and 12.0 kb, respectively. DNA was digested with *Nde*I and hybridized with the right arm (RA) probe. The fragment sizes for wild type (+/+) and EY (EY/+) alleles are 7.9 kb and 10.9 kb, respectively. (**C**) Southern blot analysis of wild type (+/+), *Ube3a*^{YFP} heterozygous (EY/+), and *Ube3a*^{YFP} homozygous tail DNA digested with *Eco*RV and probed with the LA probe. (**D**) Western blots were performed with wild type (+/+), *Ube3a*^{YFP} maternal (EY/+), and *Ube3a*^{YFP} paternal (+/EY) extracts and probed with anti-E6AP (left panel) or anti-GFP (right panel) demonstrating maternal expression of *Ube3a*^{YFP} in cerebellum. Abbreviations: E, *Eco*RV; N, *Nde*I; S, *Sph*I.

Figure 2 *Ube3a*^{YFP} undergoes preferential maternal specific expression in neurons and biallelic expression in GFAP cells lining the ventricles.

(**A**) *Ube3a*^{YFP} expression was detected in pyramidal (Py) neurons in the cortex (CTX) and the CA1 region of hippocampus when inherited through the maternal (left), but not paternal (right) germ-line. (**B**) *Ube3a*^{YFP} expression was also detected in cerebellar Purkinje cell layer (PL) and in neurons in the granular layer (GR) and molecular layer (ML), when maternally, but not paternally inherited. (**C**) Biallelic expression of *Ube3a*^{YFP} was detected in GFAP positive cells located adjacent to the lateral ventricles (external capsule cells). Expression of the *Ube3a*^{YFP} maternal allele was higher in CA3 neurons

(white arrow) compared to GFAP positive cells near the lateral ventricle. Higher magnification image of the CA1 region in the hippocampus (**D**) and cerebellum (**E**) demonstrated maternal derived *Ube3a*^{YFP} was highly expressed in neurons. E6-AP:YFP staining was most intense in nuclei but was readily detectable in cytoplasm of the cell body and in dendrites. In the cerebellum, staining was most intense in Purkinje cell nuclei but was readily detectable in the nuclei of neurons in the molecular layer (ML) and granular layer (GL). Weaker staining was detected in Purkinje cell cytoplasm and processes. (**F**) Expression of maternal *Ube3a*^{EYFP} was additionally detected in olfactory neurons. Additional abbreviations: Ec, external capsule; MC, mitral cell; YFP, anti-YFP; GFAP, anti-GFAP; CB, anti-calbindin. Scale bar A and B 100 μm, C, D, E, and F 20 μm.

Figure 3 Intracellular distribution of E6-AP:YFP to the nucleus and synapse in dissociated hippocampal neurons.

E6-AP:YFP undergoes differential intracellular trafficking to the growth cone, synapse (presynaptic and postsynaptic), and nucleus in dissociated hippocampal neurons. (**A**) Confocal images taken of *Ube3a*^{YFP} maternal derived neurons at 1, 2, 3, and 4 days *in vitro* (DIV) demonstrated that E6-AP:YFP was enriched in the nucleus (white arrowheads) and growth cones of primary elongating neurites. The ends of primary neurites were magnified to demonstrate enrichment of E6-AP:YFP (dashed boxes are expanded to panels below). (**B**) Images taken of *Ube3a*^{YFP} neurons 4 DIV stained with anti-MAP2 and anti-YFP indicated localization of E6-AP:YFP to both axons and dendrites in developing neurons. (**C**) High magnification confocal images taken of 25 DIV neurons stained with anti-synaptophysin (SYP) and anti-YFP demonstrated distinct clustering of E6-AP:YFP with synaptophysin along axons. (**D**) Along dendritic shafts, E6-AP:EYFP was diffusely distributed and was present in dendritic spines (white arrowheads). Scale bar 10 μm in **C** and **D**.

Figure 4 Loss of maternal E6-AP does not affect cerebellar Purkinje cell organization or dendritic branching. (**A**) Representative confocal images showing calbindin staining in WT and AS (maternal null) mice. Purkinje cells in AS mice show similar organization and branching compared to WT. (**B**) Quantitative confocal analysis of calbindin staining in Purkinje cell dendrites as an indirect indicator of branching. The mean calbindin fluorescence across Purkinje cell soma and dendrites was not statistically significant between WT and AS mice indicating normal Purkinje cell dendritic branching in AS mice. Abbreviation: dp, data points.

Figure 5 Abnormal dendritic spine morphology in mice with maternal deficiency for E6-AP.

AS mice exhibited abnormal dendritic spines on cerebellar, cortical, and hippocampal neurons, despite normal cellular architecture and dendritic branching. (**A**) Light micrograph images from Golgi impregnated Purkinje cell (PC), hippocampal (HP) pyramidal neurons, and cortical (CT) pyramidal neurons demonstrated AS mice had reduced dendritic spine density and an abnormal morphology in AS mice compared to WT mice. In addition, AS mice had swellings (black arrowheads) along secondary apical dendrites. (**B and C**) Dendritic spine density was significantly reduced along secondary apical dendrites in CA1 pyramidal neurons and on layer 3-5 cortical pyramidal neurons in AS mice. (**D**) The average dendritic spine length along apical dendrites in CA1 pyramidal was reduced in AS mice. Scale bar, 10 μm. Error bars are standard error of the mean. *, P = 0.03, ** P = 0.003, *** P = 0.0009.

Figure-1, Dindot et al.

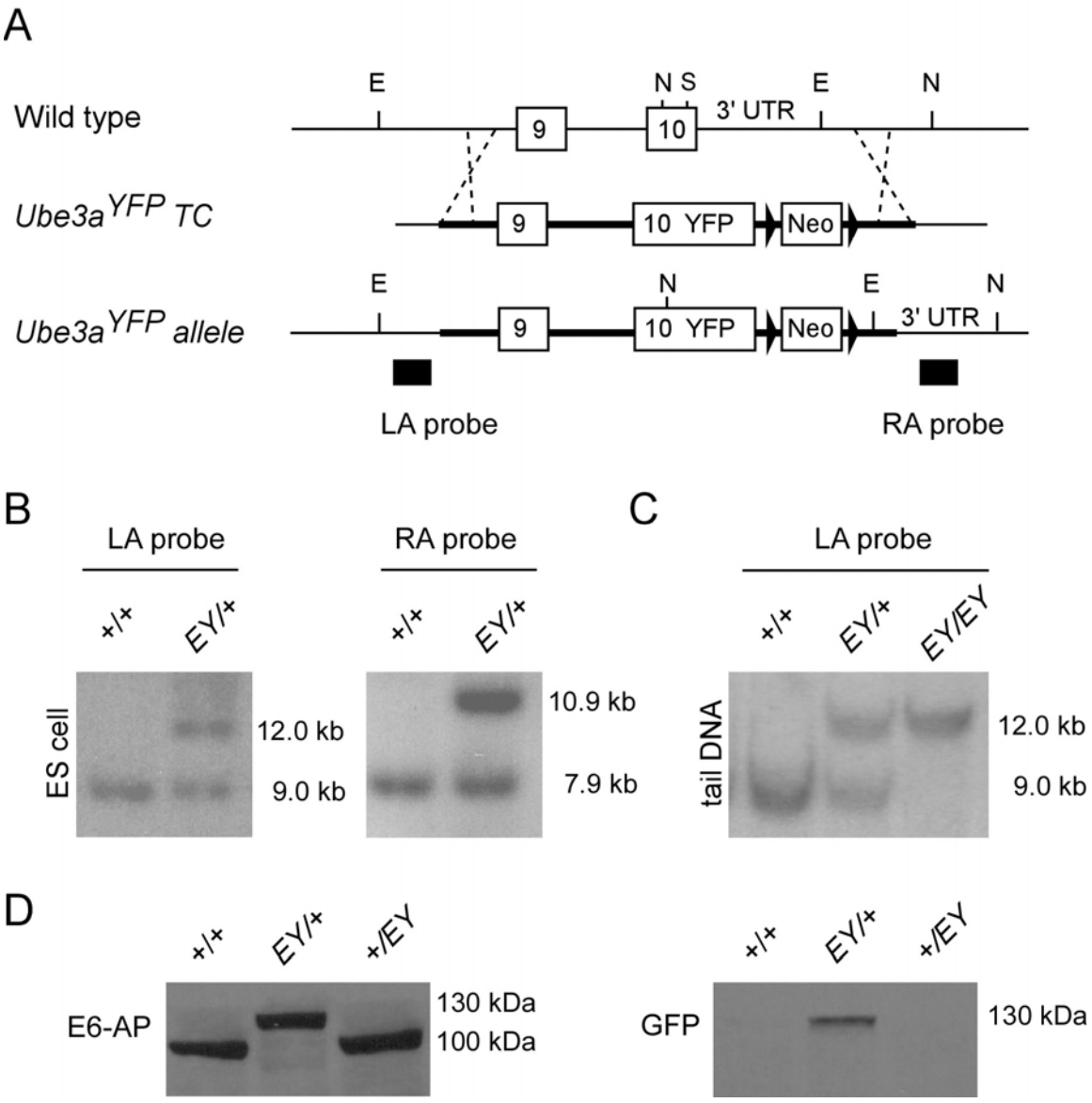

Figure-2, Dindot et al.

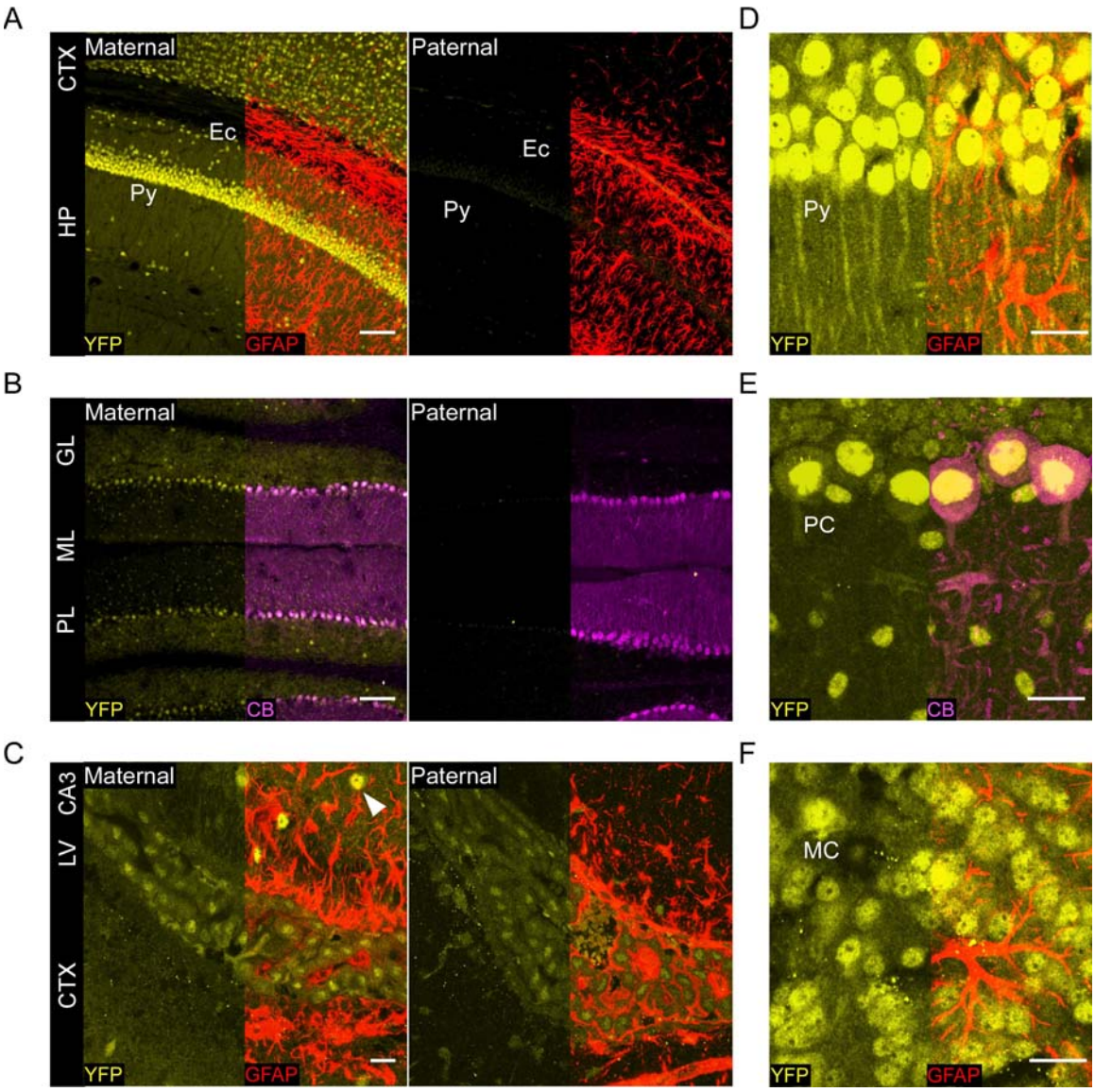

Figure-3, Dindot et al.

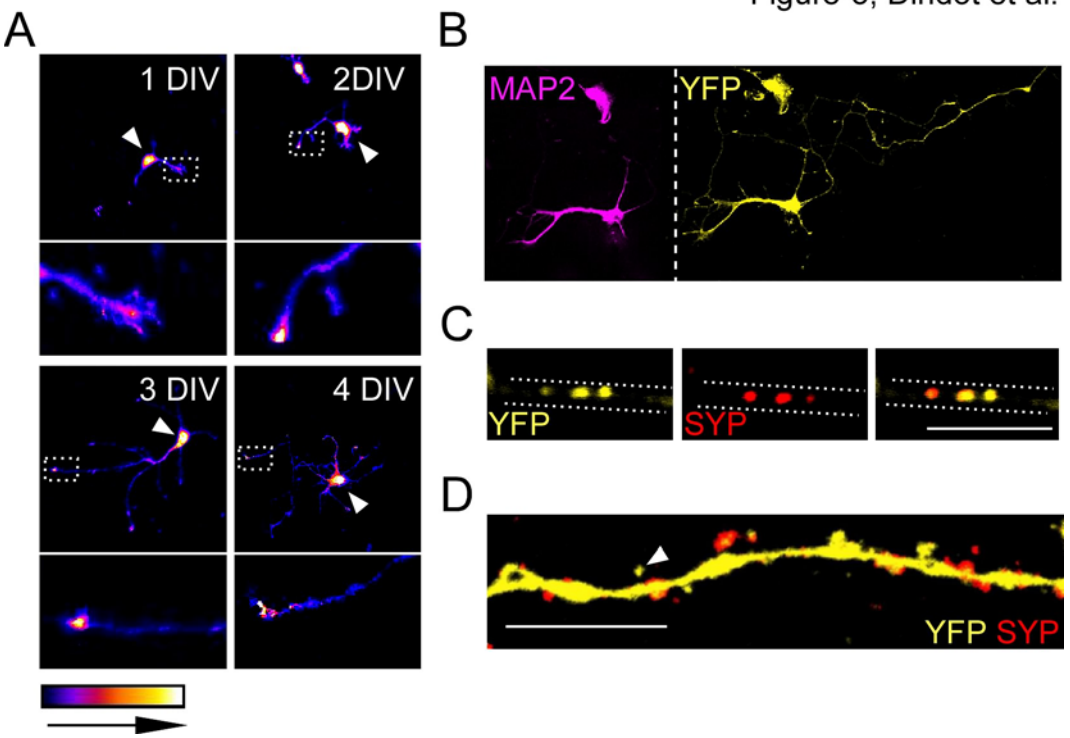

Figure-4, Dindot et al.

A

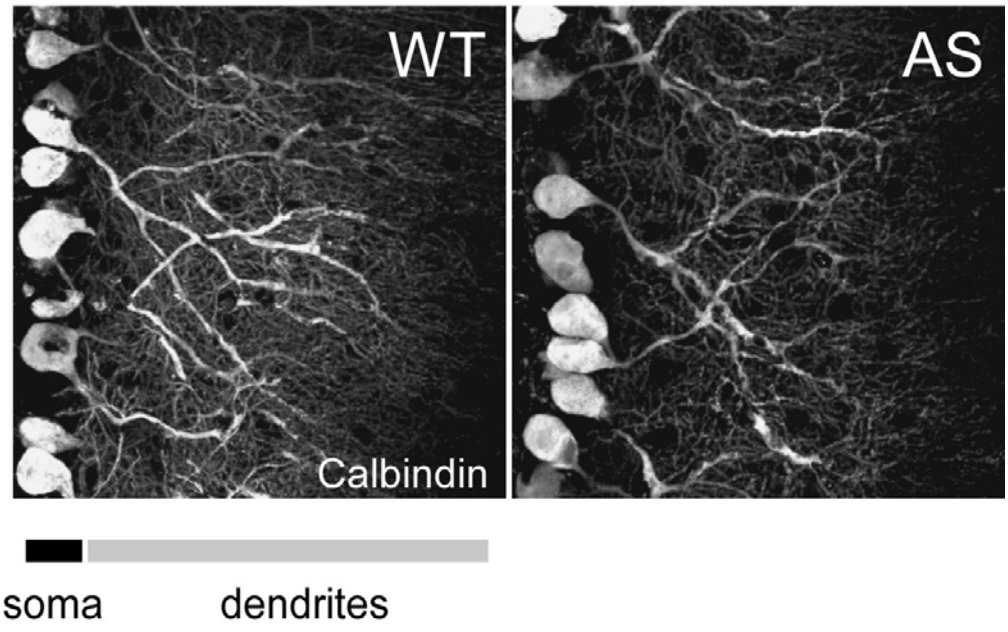

B

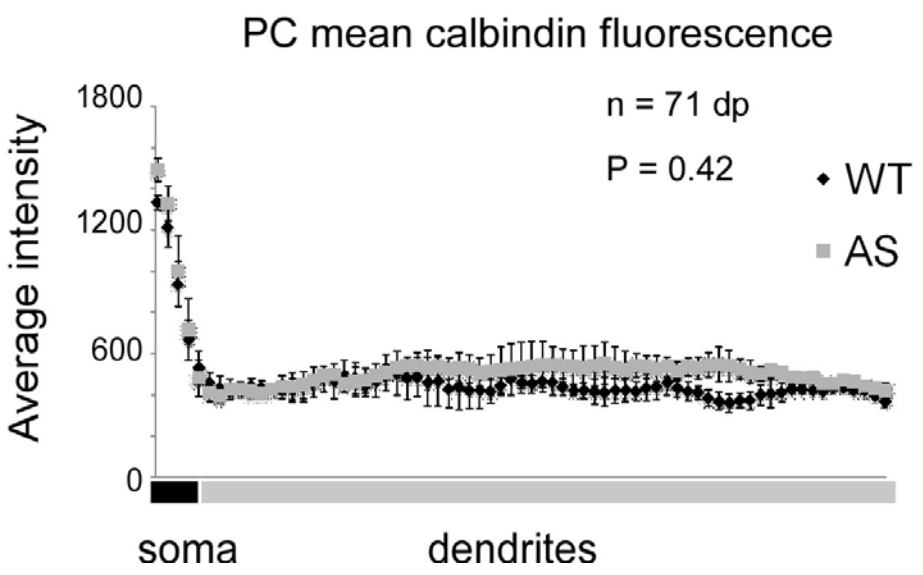

Figure-5 Dindot et al.